Thesis for the Degree of Licentiate of Philosophy

Characterization of Micro-Structures in Materials

Henrike Häbel

Division of Mathematical Statistics
Department of Mathematical Sciences
Chalmers University of Technology and University of Gothenburg
Göteborg, Sweden 2015

This work is part of the VINN Excellence Centre SuMo Biomaterials and is supported by the Swedish Governmental Agency for Innovations Systems, VINNOVA, the Knut and Alice Wallenberg Foundation, KAW, and the Swedish Foundation for Strategic Research, SSF.

Characterization of Micro-Structures in Materials
Henrike Häbel

Department of Mathematical Sciences
Chalmers University of Technology and University of Gothenburg
SE-412 96 GÖTEBORG, Sweden
Phone: +46 (0)31 772 5380

Author e-mail: henrike.habel@chalmers.se

Typeset with LaTeX.
Department of Mathematical Sciences
Printed in Göteborg, Sweden 2015

Characterization of Micro-Structures in Materials

Henrike Häbel

Department of Mathematical Sciences
Chalmers University of Technology and University of Gothenburg

Abstract

On developing the next generation sustainable soft materials, it is often crucial to understand and control their properties and function. Whereas a characterization of three-dimensional data is desirable in corresponding studies, often two-dimensional data are less time consuming to obtain. Consequently, characterizing the three-dimensional micro-structure of a material from two-dimensional data would enable efficient screening of its properties. In this work, the challenge of characterizing two different materials from two-dimensional images obtained by scanning (transmission) electron microscopy is overcome by using tools from image analysis and spatial statistics. The two different materials are a colloidal nanoparticle gel and a polymer blended film.

The characterization of the micro-structures in the materials is conducted in two main steps. First, the microscopy images are processed in order to identify the objects of interest. Second, the structures are characterized according to the objects of interest. In particular, the spatial arrangement of nanoparticles is evaluated by summary functions from spatial statistics. One such function based on the size of a cluster of particles has been developed in this project. For the pore space analysis of a polymer blended film, tools from image analysis are applied to measure and compare the shapes of pores in a statistical analysis.

The results obtained in this work, may be useful for reconstructions of the micro-structure in materials in three dimensions. Such reconstructions can be used to analyze materials, which may not yet have even been synthesized, in simulation studies without experiments involving valuable resources. In that way, new sustainable high quality products may be developed.

Keywords: Clustering, colloidal nanoparticle gels, image analysis, mass transport, point pattern, polymer blended films, pore shape.

List of appended papers

Paper I Nordin, M.; Abrahamsson, C.; Hamngren Blomqvist, C.; **Häbel, H.**; Röding, M., Olsson, E., Nydén, M., Rudemo, M.. Estimation of mass thickness response of embedded aggregated silica nanospheres from high angle annular dark-field scanning transmission electron micrographs. *Journal of Microscopy*, 253(2):166-170, 2014.

Paper II **Häbel, H.**; Särkkä, A.; Rudemo, M.; Hamngren Blomqvist, C., Olsson, E., Abrahamsson, C.; Nordin, M.. From static micrographs to particle aggregation dynamics in three dimensions. *Manuscript*.

Paper III **Häbel, H.**; Andersson, H.; Jansson A.; Olsson, E.; Larsson, A.; Särkkä, A.. Characterization of pore structure of polymer blended films used for controlled drug release. *Manuscript*.

My contribution to the appended papers:

Paper I: I validated the developed log-likelihood method for the estimation of mass thickness response in a simulation study.

Paper II: I co-developed the particle detection algorithm, developed a new summary function for cluster size and conducted all statistical analyses. I also did most of the writing of the publication.

Paper III: I co-developed the polymer phase segmentation, conducted all statistical analyses and I did most of the writing of the publication.

Publication written within the Center for Applied Mathematics and Statistics not included in this thesis:

Karimi, M.; Hedner, J.; **Häbel, H.**; Nerman, O.; Grote, L.. A sleep apnea related excess risk of motor vehicle accidents in the Swedish Traffic Accident Registry is reduced by CPAP - a retrospective cohort study. *Sleep*, Epub, 2014.

Acknowledgments

First of all, I would like to thank Aila Särkkä and Mats Rudemo for their great supervision and commitment to my research project. I especially appreciate our team dynamics.

Furthermore, I am grateful for the inspiring interdisciplinary research group created within SuMo Biomaterials and the KAW/SSF project group. I have always enjoyed the fruitful discussions and chemistry lessons with my collaborators and colleagues: Christoffer Abrahamsson, Helene Andersson, Charlotte Hamngren Blomqvist, Anna Jansson, Anette Larsson, Niklas Lorén, Mariagrazia Marucci, Matias Nordin, Eva Olsson, Holger Rootzén and many more.

My thanks go also out to my fellow Ph.D. students who are not just colleagues, but friends. Especially, I would like to thank Kristin Kirchner for a little bit of home abroad, Anna Olsson for lovely lunches, Farzaneh Safavimanesh for her openness and kindness and Mariana Pereira, Viktor Jonsson and Fredrik Boulund for making me feel welcome from the beginning.

Last, but not least, I would like to thank my family and friends for their love and support as well as Gothenburg GAA for its contribution to my work-life balance.

Henrike Häbel
Gothenburg, March 20, 2015

Important abbreviations

CLSM	Confocal laser scanning microscopy
DLCA	Diffusion limited cluster aggregation
EC	Ethyl cellulose
HAADF	High-angular annular dark field
HPC	Hydroxypropyl cellulose
M_w	Molecular weight
RLCA	Reaction limited cluster aggregation
SEM	Scanning electron microscopy
STEM	Scanning transmission electron microscopy
w/w	Weight/weight

Contents

1 Introduction

Current microscopy techniques allow us to obtain images of structures of materials on a scale of a thousandth of a millimeter or even smaller. These images enable a characterization of micro-structures and therewith open up opportunities to understand and control material properties and functions. For instance, understanding the relationship between mass transport through and the micro-structures of a material is of great importance in various fields ranging from drug development over food processing to chromatography. Ideally, three-dimensional structures should be studied. However, obtaining three-dimensional data by microscopy is very time consuming and has usually more limitations than taking two-dimensional images. The aim of this work is to overcome the challenge of characterizing three-dimensional structures from two-dimensional images by using tools from image analysis and summary functions from spatial statistics on the example of two different soft materials.

The first material is a colloidal silica nanoparticle gel, where the pore structure is determined by the arrangement of the nanoparticles after aggregation. Silica gels can serve as test beds for mass transport since they have well known gelation properties. If only two-dimensional images are available, a three-dimensional reconstruction of the particle positions is important for mass transport simulations through the pore structure. One aim in this work is to understand how silica nanoparticles aggregate and, hence, how the pore structure is formed.

The second material consists of phase-separated polymer blends forming a film which can be used as a pharmaceutical coating for oral controlled drug release formulations such as pellets. The main question discussed here is what characteristics of the pore structure affect the water permeability of the film. Water permeability through the studied films is equivalent to diffusion through them.

Both materials are introduced in Section 2 after a short description of mass transport and diffusion. Since the characterization of the materials was conducted using images obtained by microscopy techniques, a brief overview of how the given data are obtained is presented in Section 2.4. Subsequently, an introduction to the tools used from image analysis is given in Section 3 and from spatial statistics in Section 4. Finally, the papers appended in this thesis are introduced in Section 5, before some plans for future work are outlined in Section 6.

2 Material properties and structures

In this section, the materials and data studied in this work are presented. Since mass transport is of certain interest and the diffusion of particles plays an important role in the aggregation of silica, an introduction to mass transport and diffusion is given first.

2.1 Mass transport and diffusion

Mass transport refers to the net transport of mass like water from one location to another. Diffusion describes the net transport of mass from regions of relatively high concentrations c_1 to regions with relatively low concentration c_2 by random molecular motion in a thin sample of thickness h with diffusion coefficient

$$\mathrm{D} = \frac{h}{\mathrm{A}(c_1 - c_2)} \frac{\partial m}{\partial t}.$$

Here, A refers to the surface area of the sample and $\frac{\partial m}{\partial t}$ denotes the mass transport rate along the cross-section direction of the sample (Cussler, E.L., 1997, p.16 ff.). In Einstein (1905) a differential equation for the diffusion of n particles is given by

$$\frac{\partial m}{\partial t} = D \frac{\partial^2 m}{\partial x^2},$$

with solution

$$m(x,t) = \frac{n}{\sqrt{4\pi \,\mathrm{D}\, t}} \exp\left(-\frac{x^2}{4\,\mathrm{D}\,t}\right)$$

where $m(x,t)dx$ gives the number of particles whose x-coordinate changed one unit between x and $x + dx$ in the time interval $[0,t]$. The corresponding mathematical model for a particle diffusing in $\mathbb{R}^d$ is often referred to as Brownian motion which is described by a time-continuous stochastic process $\{B(t)\}_{t\geq 0}$, $B(t) = (B^1(t), \ldots, B^d(t))$ with the following properties (Grimmett and Stirzaker, 2001, p. 514 ff.)

- $B(0) = \mathbf{0}$,
- $B^1, \ldots, B^d$ are independent and identically distributed processes,
- $B^1(s+t) - B^1(s) \sim \mathcal{N}(0, \sigma^2 t) \quad \forall s, t \geq 0$,
- B^1 has independent increments.

Here, $\sqrt{\bar{x}^2} = \sqrt{\sigma^2 t} = \sqrt{2\,\mathrm{D}\,t}$ corresponds to the expected shift of a particle along the x-axis (Einstein, 1905).

2.2 Colloidal nanoparticle gels

A widely used colloid is milk which consists of insoluble milk proteins dispersed within a water-based solution. On destabilizing the protein dispersion by lowering the pH, for instance, that is by making the milk more acidic, the proteins aggregate and set yoghurt is obtained (de Kruif et al., 1995). A simpler colloidal system is formed by silica nanoparticles dispersed in a water-based solution. Silica dispersions are often used to

study colloidal aggregation and gelation as in Schantz Zackrisson et al. (2006). Figure 1 schematically shows the gelation process. At the beginning (A) there is a stable solution such as milk or silica particles dispersed in a water-based solution. After destabilization of the dispersion by addition of salt, for example, the particles start to aggregate and form clusters (B). The gelation is completed when all particles have aggregated into one large cluster (C). Consequently, understanding step B is most important when studying colloidal aggregation.

There are two universal limiting regimes used to describe such aggregation, diffusion limited and reaction limited cluster aggregation (Schantz Zackrisson et al., 2006). In both regimes particles diffuse according to Brownian motion. In diffusion limited cluster aggregation, particles aggregate immediately after collision and form clusters with time. In the more general reaction limited regime, interactions between particles may prohibit their aggregation and prolong the formation of clusters. A probability of aggregation can be introduced to distinguish between the different aggregation processes; the probability of aggregation is one in the diffusion limited regime and smaller than one otherwise. In this work, the probability of aggregation is studied on an aggregated network of colloidal silica nanoparticles with a diameter of around 20 nm. The gel was formed from a water-based silica dispersion (AkzoNobel Pulp and Performance Chemicals, Sweden) and images of the micro-structure were obtained by scanning transmission electron microscopy, where particles in a 90 nm thin gel layer are projected on an images as shown in Figure 1 D.

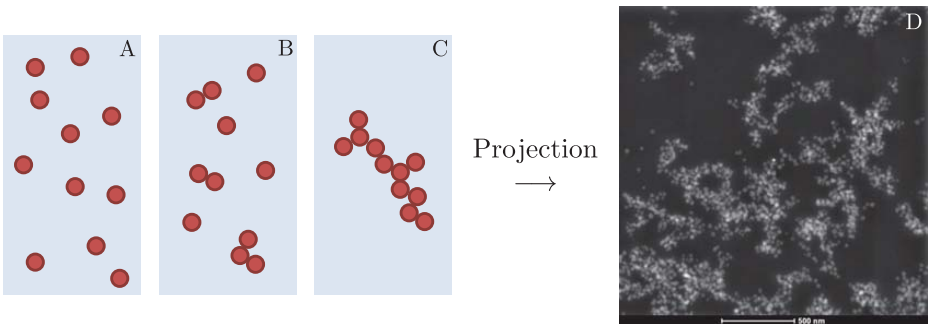

Figure 1: Schematic illustration of aggregation of colloidal particles in a stable dispersion (A), forming clusters after destabilization (B) and finally a gel (C) and projection obtain by scanning transmission electron microscopy of a gel sample (D).

2.3 Polymer blended films

Polymers are formed by molecules featuring repetitions of consecutive units called monomers. Here, a consecutive unit refers to the smallest regularly repeating unit which completely describes the macromolecular chain. There are many different kinds and

groups of polymers, but especially bio-based polymers produced from renewable resources gain global importance. Cellulose, for instance, is a bio-based polymer extracted from plant fibers, which has long been used to build materials such as papyrus in ancient Egypt (Klemm et al., 2005).

In this work, two cellulose derivatives, namely ethyl cellulose (EC) and hydroxypropyl cellulose (HPC), are used to form semi-water-soluble films that can be used as pharmaceutical controlled release coatings. Here, free films are studied since they are convenient for screening properties of such coatings. The basis for a film is a blend of EC and HPC dissolved in ethanol. The resulting solution is sprayed onto a rotating Teflon drum by a moving spraying nozzle using a heated air flow as shown in Figure 2. The spraying of the films takes place in a modified fluidized-bed chamber originally designed for coating pellets. While drying, the ethanol evaporates which induces phase-separation of the at first homogeneously mixed EC and HPC phase. As a consequence, EC-rich and HPC-rich bicontinuous phases form. This process is called spinodal decomposition and is frozen by a high film viscosity which is reached at a certain ethanol concentration (Marucci et al., 2013). Whereas EC is not soluble in water or in the gastrointestinal tract, HPC may act as a pore former when dissolved in water (Sakellariou and Rowe, 1995). As a result, pores are created in the HPC-rich phase.

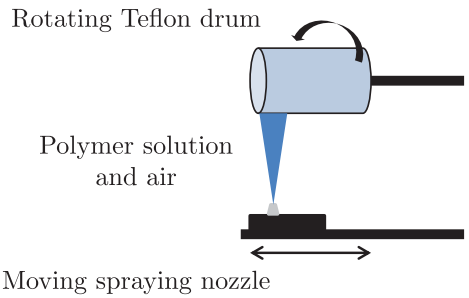

Figure 2: Schematic illustration of the spraying process of free polymer blended films.

There are several factors influencing the formation of the micro-structure such as film processing parameters, polymer contents and viscosity. Viscosity, meaning the polymers resistance to flow, depends on the degree of entanglements of the macromolecular chains, which, in turn, depends on the molecular weight of the polymer (Cowie, 1991, p. 256). Here, two HPC viscosity grades were used to produce two different films. These polymer blended solutions contained 70% EC (w/w, Dow Wolff Cellulosics GmbH, Germany) and 30% HPC (w/w) in two different viscosity grades, HPC-SL and HPC-L (Nisso HPC, Nippon Soda Co. Ltd, Japan). Images of the surface of film cross-sections were obtained by scanning electron microscopy and one example for each HPC viscosity grade is presented in Figure 3. Prior to imaging, HPC was dissolved in water and the remaining EC was coated by a thin gold layer in order to increase the signal.

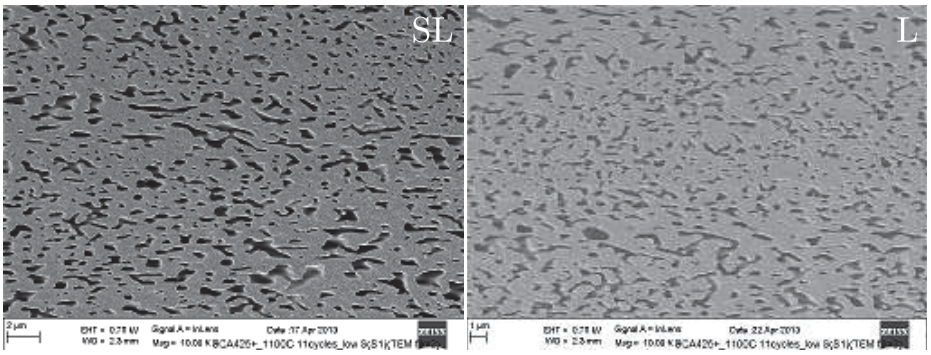

Figure 3: Cross-sections of EC/HPC-SL (left) and EC/HPC-L (right) polymer blended films. The EC-rich phase is depicted in gray and the pores formed after dissolving of the HPC-rich phase are black.

2.4 Microscopy

All data provided for this study were obtained by microscopy techniques built on a focused electron beam as schematically presented in Figure 4 (Pennycook et al., 2006). In scanning transmission electron microscopy, an electron beam scans over and electrons are transmitted through a sample while a detector collects the response. The sample has to be very thin in order to obtain good images. In scanning electron microscopy, the detector collects the signal from reflected electrons.

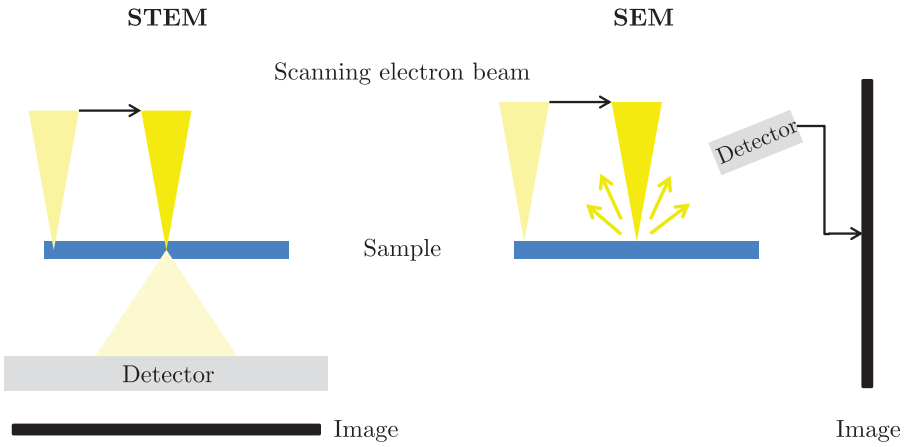

Figure 4: Schematic illustration of scanning transmission electron microscopy (STEM) and scanning electron microscopy (SEM).

3 Image analysis

Tools from image analysis were used to identify objects of interest by image segmentation as presented in Section 3.1. Section 3.2 presents further manipulations to the morphology of the objects. Objects of interest can also be found by circle detection as presented in Section 3.3. In the following, an image is regarded as a matrix $I = (I_{i,j})_{i=1,\dots,M;\ j=1,\dots,N}$, where each entry $I_{i,j}$ represents a pixel value on a gray-scale.

3.1 Image filtering and segmentation

An image may have to be enhanced prior to and even after segmentation. For example, filtering can be used to handle noise, detect edges or to smoothen an image. Filtering involves a transformation of the image I using matrix operations often depending on a specified neighborhood around each pixel. In particular, an $n \times n$ neighborhood for $n \in \mathbb{N} = \{1, 2, \dots\}$ corresponds to an $n \times n$ matrix

$$w = (w_{k,\ell},\ \ell = -p, -p+1, \dots, p;\ k = -p, -p+1, \dots, p),$$

for $p = \lfloor \frac{n}{2} \rfloor$, where $\lfloor \cdot \rfloor$ denotes the floor function. A new, filtered image is obtained by

$$I_{i,j}^{new} = \sum_{k=-p}^{p} \sum_{l=-p}^{p} w_{k,\ell} I_{i+k,j+\ell}.$$

For a simple averaging filter, equal weights $w_{k,l} = \frac{1}{n \cdot n}$ are used. In this work, a more complex pixelwise adaptive Wiener filtering was used for Gaussian white noise reduction. This transformation is based on local estimates for the mean μ and the variance σ^2. The noise variance σ_n^2 is estimated by taking the average over all locally estimated variances. The transformed image I^{new} is obtained by setting

$$I_{i,j}^{new} = \hat{\mu} + \frac{\hat{\sigma}^2 - \hat{\sigma}_n^2}{\hat{\sigma}^2}(I_{i,j} - \hat{\mu}),$$

where $\hat{\mu}$ and $\hat{\sigma}^2$ refer to the locally estimated mean value and variance, respectively, and $\hat{\sigma}_n^2$ is the estimated noise variance. More details on filters can be found in Glasbey and Horgan (1995, Chapter 3).

Image segmentation is used to classify and discriminate regions of different pixel values in an image. Since the result is a binary image with black background and white objects, image segmentation is also called binarization. Selecting an appropriate threshold for the binarization is crucial. A commonly used method applied to select a threshold is Otsu's method (Otsu, 1979). This method is based on the histogram of the pixel values at L different levels, where the optimal threshold k^* corresponds to the value which minimizes the variance of pixel values below and above it. In particular, the histogram is divided into two classes with levels $[1, \dots, k]$ in the first class and $[k+1, \dots, L]$ in the second

class for some threshold k. Let $\sigma_B^2(k)$ denote the between-class variance, then the optimal threshold k^* can be found by using that

$$\sigma_B^2(k^*) = \max_{1 \le k < L} \sigma_B^2(k).$$

3.2 Morphological operations

The most standard morphological operations are erosion and dilation with a structure element S moved along certain reference pixels collected in a set A. These operations can be used to remove small objects or enlarge the contrast of an image, for example. Let the group of pixels $S_{(i,j)}$ be the structure element S placed with its reference pixel at (i, j). Then the erosion of A by S can be defined as

$$A \ominus S = \{(i, j) : \ S_{(i,j)} \subset A\}$$

and the dilation of A by S is given by

$$A \oplus S = (A^c \ominus S)^c,$$

where A^c denotes the complement of A. If A is the set of pixels of objects that are set to one after segmentation, A^c is the set of pixels set to zero (Glasbey and Horgan, 1995, Chapter 5). Figure 5 gives an example for erosion (C) and dilation (D) with a spherical structure element S with a diameter of 3 pixels.

Sequential thinning of the set A is another useful morphological operation and can be used for the shape characterization of objects. For example, A can be thinned until a skeleton is obtained. A skeleton is the union of minimally connected line segments with the thickness of one pixel. In the thinning algorithm as for instance presented in Lam, L. and Lee, S.W. (1992), pixels from the boundary of objects are removed while preserving the number of objects and holes in an image. Figure 5 D shows an example of a dilated skeleton.

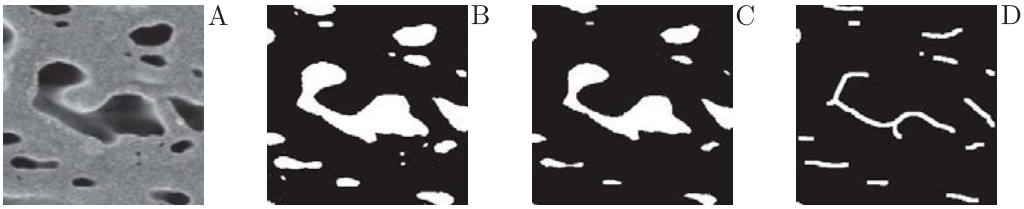

Figure 5: Example of an original gray-scale image A of size 250 by 250 pixels, B after segmentation and C after erosion by a pixelized disk with a diameter of 3 pixels. D shows the skeleton of the eroded image C dilated by the same structure element.

3.3 Detection of circular objects

Often specific shapes have to be detected in an image, for instance circular objects. For this purpose, the circular Hough transform can be used (Atherton and Kerbyson, 1999). Let (x_0, y_0) denote the two-dimensional position of a circle center. Then a circle with radius $R \in \mathbb{R}^2$ can be represented as the following system of equations

$$\begin{aligned} x &= x_0 + R\cos(\alpha) \\ y &= y_0 + R\sin(\alpha), \end{aligned}$$

where x and y trace the circle perimeter according to the angle $\alpha \in [-\pi, \pi]$. An alternative representation yields $R^2 = (x - x_0)^2 + (y - y_0)^2$. The Hough transform transforms the (x, y)-space to a three-dimensional parameter space (x_0, y_0, R). Candidates for points on the circle perimeter are pixels with a large gradient magnitude, which is calculated by the partial gradient images for column vectors $I(j),\ j = 1, \ldots, N$ and row vectors $I(i),\ i = 1, \ldots, M$

$$\begin{aligned} \frac{\partial I(j)}{\partial x} &= 0.5\left(I(j+1) - I(j-1)\right), \\ \frac{\partial I(i)}{\partial y} &= 0.5\left(I(i+1) - I(i-1)\right). \end{aligned}$$

The gradient magnitude is given by $\sqrt{\frac{\partial I}{\partial x}^2 + \frac{\partial I}{\partial y}^2}$ and the gradient direction by $\frac{180}{\pi}\arctan\left(-\frac{\partial I}{\partial y}, \frac{\partial I}{\partial x}\right)$. An example of a gradient magnitude and a gradient direction image is presented in Figure 6 together with an example of detected spheres.

In order to detect circular objects, a circle with radius R is drawn around each candidate point and the points at the intersections are used as estimates for circle centers. This method can be extended to a range of radii $R_{min} \leq R \leq R_{max}$, see for instance Atherton and Kerbyson (1999).

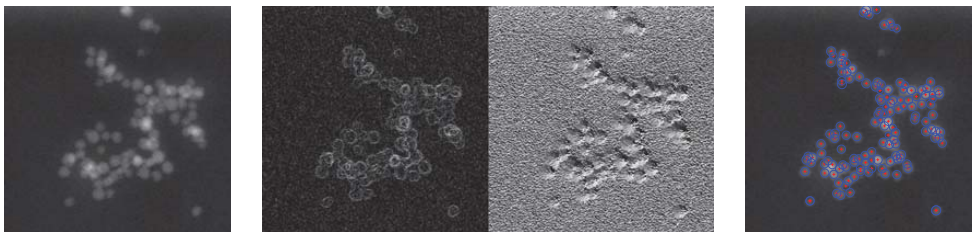

Figure 6: Example of gray-scale image (left) and corresponding gradient magnitudes (middle left) as well as directions (middle right) and the result of the particle detection algorithm (right).

4 Point processes

This section presents basic definitions and characteristics of random spatial point processes which are fundamental to the spatial statistical analysis conducted in this work. Henceforth, $\mathcal{B}(\mathbb{R}^d)$ denotes the family of all Borel sets on $\mathbb{R}^d$ and $\mathcal{B}_0(\mathbb{R}^d)$ refers to the family of all bounded Borel sets on $\mathbb{R}^d$. The d-dimensional Lebesgue measure ν_d is used to quantify geometric properties.

4.1 Basic definitions

Random spatial point processes provide mathematical models for objects randomly distributed on the plane or in space. Point process models can be used to characterize the spatial arrangement of point patterns arising from the objects of interest and may contribute to solving problems in diverse fields as, for instance here, in material science. Point processes can be interpreted either as random sets of discrete points or as random counting measures (Stoyan et al., 1995, p. 99 ff.).

Definition 4.1 (Point process)**.** A sequence $X = \{X_i\}_{i\in\mathbb{N}}$ of random vectors $X_i : \Omega \to \mathbb{R}^d \cup \{\infty\}$ on some probability space $(\Omega, \mathcal{A}, \mathbb{P})$ is called a *point process* if

$$X(B) = h_0(X \cap B) < \infty \quad \forall\, B \in \mathcal{B}_0(\mathbb{R}^d),$$

where $X(B)$ gives the number of points of the process in the set B. If

$$\mathbb{P}(X_i \neq X_j) = 1 \quad \forall\, i, j \geq 1,\ i \neq j,$$

X is called a *simple* point process.

Let $\mathbf{N}$ denote the family of all locally finite counting measures $\boldsymbol{x}$ and $\mathcal{N}$ be the smallest σ-algebra on $\mathbf{N}$ such that the mapping $\boldsymbol{x} \mapsto \boldsymbol{x}(B)$ is $(\mathcal{N}, \mathcal{B}(\mathbb{R}))$-measurable for every bounded set $B \in \mathcal{B}(\mathbb{R}^d)$. Then, a point process X is a measurable mapping of a probability space $(\Omega, \mathcal{A}, \mathbb{P})$ into $(\mathbf{N}, \mathcal{N})$ and generates a distribution P_X of X on $(\mathbf{N}, \mathcal{N})$. Consequently, X can be seen as a random choice of a sequence $\boldsymbol{x} \in \mathbf{N}$ of points in $\mathbb{R}^d$.

The expectation of a point process is called the intensity measure and is defined as follows.

Definition 4.2 (Intensity measure)**.** A measure $\Lambda : \mathcal{B}(\mathbb{R}^d) \to [0, \infty)$ is called the *intensity measure* of a point process X if

$$\Lambda(B) = \mathbb{E}[X(B)] = \int_{\mathbf{N}} \boldsymbol{x}(B) P_X(d\boldsymbol{x}) \quad \forall B \in \mathcal{B}(\mathbb{R}^d).$$

Henceforth, the intensity measure is assumed to be locally finite. Furthermore, the probability distribution of a point process P_X or the point process X itself is here assumed to be stationary and isotropic.

Definition 4.3 (Stationarity)**.** A point process X is called *stationary* or *invariant under translation* if

$$P_X(A) = P_X(A_{-x}) \quad \forall A \in \mathcal{N},\ \forall x \in \mathbb{R}^d$$

for $A_x = \{\boldsymbol{x} \in \mathbf{N} :\ \boldsymbol{x}_{-x} \in A\}$ for $A \in \mathcal{N}$, where $\boldsymbol{x}_{-x}$ denotes the random sequence of points $\boldsymbol{x}$ translated by the vector x.

Definition 4.4 (Isotropy)**.** A point process X is called *isotropic* or *rotation invariant* if

$$P_X(A) = P_X(\delta A) \quad \forall A \in \mathcal{N},$$

for every rotation $\delta : \mathbb{R}^d \to \mathbb{R}^d$ around the origin and $\delta A = \{\boldsymbol{x} \in \mathbf{N} :\ \delta^{-1}\boldsymbol{x} \in A\}$ for $A \in \mathcal{N}$.

For stationary point processes we obtain the following result which also defines the expected number of points of X per unit area.

Theorem and Definition 4.1. *Let X be a stationary point process in $\mathbb{R}^d$ and $B \in \mathcal{B}_0(\mathbb{R}^d)$, then*

$$\mathbb{E}[X(B)] = \lambda \nu_d(B)$$

for some constant $\lambda \in [0, \infty)$. λ is called the intensity *of the point process X.*

It can be useful to condition on a point of X lying at a fixed position when studying local properties. In order to assess only those points of a stationary point process X having a certain local characteristic $A \in \mathcal{N}$, the Palm distribution P_o at a typical point o of X can be used.

Definition 4.5 (Palm distribution)**.** Let X be a stationary point process with intensity $\lambda \in (0, \infty)$. Then the *Palm distribution* P_o is defined on $(\mathbf{N}, \mathcal{N})$ as

$$P_o(A) = \int \sum_{x \in \boldsymbol{x} \cap B} \frac{\mathbb{I}(\boldsymbol{x}_{-x} \in A) P_X(d\boldsymbol{x})}{\lambda \nu_d(B)} \quad \forall\ A \in \mathcal{N}$$

for arbitrary $B \in \mathcal{B}(\mathbb{R}^d)$ with $\nu_d(B) > 0$, where $\mathbb{I}(\cdot)$ is the indicator function.

One of the most important stationary point processes is the homogeneous Poisson process which underlies many other point processes and often serves as a reference model with completely randomly distributed points.

Definition 4.6 (Poisson process)**.** X is called a *Poisson process* if it satisfies the following properties.

(i) $X(B)$ is Poisson distributed with mean $\Lambda(B)$ for all $B \in \mathcal{B}_0(\mathbb{R}^d)$

(ii) If $B_1, \ldots, B_k \in \mathcal{B}(\mathbb{R}^d)$, $B_i \cap B_j = \emptyset$, $i, j \geq 1$, $i \neq j$, then $X(B_1), \ldots, X(B_k)$ are independent for arbitrary $k \in \mathbb{N}$.

If the Poisson process X is stationary then $\Lambda(B) = \lambda \nu_d(B)$ holds according to Theorem 4.1 and it is called the *homogeneous Poisson process* with intensity $\lambda \in [0, \infty)$.

4.2 Summary characteristics

Often point patterns are divided into three groups: completely spatially random or Poisson patterns with no interaction between the points, clustered patterns and regular patterns. In order to characterize the arrangement of points, summary functions of distance r can be used. This section introduces the summary characteristics considered in this work assuming stationary and isotropic point processes with intensity $\lambda > 0$.

4.2.1 First-order characteristics

The intensity measure $\Lambda(B) = \mathbb{E}[X(B)]$ is an example of first-order characteristics. Another first-order characteristic is the empty space function $F : [0, \infty) \longrightarrow [0, 1]$, which gives the distribution of the distance from an arbitrary point $x \in \mathbb{R}^d$ to the nearest point in X. Considering the probability that a ball $b(x, r)$ centered at an arbitrary point $x \in \mathbb{R}^d$ with radius r does not contain any point of X, a cumulative distribution as a function of radius r can be obtained

$$F(r) = 1 - \mathbb{P}(X(b(x, r)) = 0) \quad \forall r \geq 0.$$

The distribution of the distance from a typical point o in X to its nearest neighbor in X is summarized by the nearest neighbor distance distribution $G : [0, \infty) \longrightarrow [0, 1]$. $G(r)$ is defined using the result that the distance is smaller than r if and only if there is at least one other point in a ball with radius r centered around o given that there is a point at o.

$$G(r) = P_o(\boldsymbol{x} \in \mathbf{N} : \ \boldsymbol{x}(b(o, r)) > 1) = 1 - P_o(\boldsymbol{x} \in \mathbf{N} : \ \boldsymbol{x}(b(o, r)) = 1) \quad \forall r \geq 0.$$

4.2.2 Second-order characteristics

A common second-order characteristic is Ripley's K-function $K : [0, \infty) \to [0, \infty]$ also known as the second reduced moment function. Therefore, $\lambda K(r)$ gives the expected number of points within a ball $b(o, r)$ centered at a typical point o of X with radius r without counting o itself, in expression

$$K(r) = \frac{1}{\lambda}\mathbb{E}_o[X(b(o, r) \setminus \{o\})] = \frac{1}{\lambda}\int_{\mathbf{N}} \boldsymbol{x}(b(o, r) \setminus \{o\}) P_o(d\boldsymbol{x}) \quad \forall r \geq 0.$$

A variance stabilizing transformation of the K-function, is given by the L-function $L : [0, \infty) \to [0, \infty)$ defined as

$$L(r) = \sqrt{\frac{K(r)}{\pi}} \quad \forall\ r \geq 0.$$

The pair-correlation function $g : [0, \infty) \longrightarrow [0, \infty]$ is a normalized transform of the derivative of the K-function given by

$$g(r) = \frac{\frac{dK(r)}{dr}}{h_{d-1}(\partial b(o, r))},$$

where h_{d-1} quantifies the surface of a ball $b(o,r)$. Hence, for $d=2$, h_1 gives the length of the perimeter of the circle $b(o,r)$.

4.2.3 Higher-order characteristics

In order to describe the interpoint behavior of a point process on a higher-order, the behavior between more than two points can be taken into account. A third-order characteristic, the clustering function, is introduced in Rajala (2010). In particular, the clustering function $c:[0,\infty) \longrightarrow [0,1]$ sets the number of observed triplets in a ball $b(o,r)$ in relationship to the theoretical number of possible triplets. Let $ne(o) = X \cap (b(o,r) \setminus \{o\})$, then

$$c(r) = \int_{\mathbf{N}} c_{o,r} P_o(d\boldsymbol{x}) \quad \forall r \geq 0$$

where

$$c_{o,r} = \frac{\sum_{x,y \in ne(o)} \boldsymbol{x}(b(o,r) \cap b(x, \|x-y\|) \setminus \{o\})}{\frac{1}{2}(\delta(o)^2 - \delta(o))} \cdot \mathbb{I}(\delta(o) > 2)$$

and

$$\delta(o) = \boldsymbol{x}(b(o,r) \setminus \{o\}).$$

On joining several points of a planar point process in a cluster, another higher-order characteristic can be defined for the mean cluster size based on the diameter of a cluster

$$D = 2\sqrt{\frac{1}{2n_k^2} \sum_{x \in \mathcal{C}_k} \sum_{y \in \mathcal{C}_k} \|x-y\|^2},$$

where n_k is the number of particles in a cluster $\mathcal{C}_k$. D is also called the diameter of gyration (Khan et al., 2014). The mean cluster size function $M:[0,\infty) \longrightarrow [0,\infty)$ is defined as

$$M(r) = \mathbb{E}(D_r) \quad \forall r \geq 0$$

where

$$D_r = 2\sqrt{\frac{1}{2n_{r,k}^2} \sum_{x \in \mathcal{C}_{r,k}} \sum_{y \in \mathcal{C}_{r,k}} \|x-y\|^2}$$

for a cluster $\mathcal{C}_{r,k} \in \mathbb{R}^2$ including $n_{r,k}$ points. The cluster region $\mathcal{C}_{r,k}$ is here defined by geometric graphs (Penrose, 2003) placing an edge between two points if the distance between two points $\|x-y\|^2$ is smaller than r. As a result, each $\mathcal{C}_{r,k}$ is formed by a set of points connected in the graph as depicted in Figure 7.

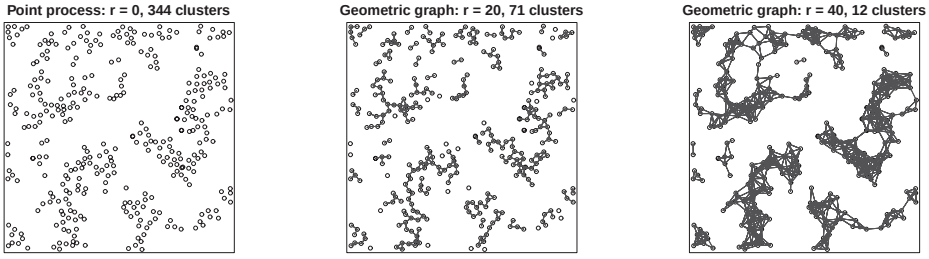

Figure 7: Definition of clusters using a geometric graph with edge length $r = 0$ (left), $r = 20$ (middle) and $r = 40$ (right) in a 600×600 observation window.

4.2.4 Estimation of summary functions

Whereas a point process X is defined on whole $\mathbb{R}^d$, point patterns can only be observed in bounded observation windows $W \subset \mathbb{R}^d$. Since the missing observations outside W may affect the estimation of summary functions, their estimators have to incorporate some edge correction. There are several methods available for dealing with edge effects as can be found in Stoyan et al. (1995, p. 133 ff.), Illian et al. (2008, p. 228 ff.) and in many further publications. In the articles appended in this thesis, edge corrected estimators are given to those summary functions that are used.

5 Summary of appended papers

In this section, the three appended papers are introduced in the context of this thesis. Since the emphasis in all papers is on the developed methods, the main components of each method are presented. Furthermore, the main results of each work are highlighted.

5.1 Paper I and II: Colloidal nanoparticle gels

Paper I: Estimation of mass thickness response of embedded aggregated silica nanoparticles from high angle annular dark-field scanning transmission electron micrographs

High angle annular dark-field scanning transmission electron micrographs allow for two-dimensional projections which still contain information about the structure along the projected axis of three-dimensional samples. The motivation for this work was to find a method for estimating the mass thickness response from such micrographs on the example of nano sized (20 nm) silica particle gels. The estimation is based on the relationship between the mass thickness of the silica and the intensity observed at each pixel of an input micrograph image. Here, the intensity is modeled as a power function of the mass thickness with additive zero-mean Gaussian noise. The parameters involved were estimated by maximizing the log-likelihood while iterating the positions of artificial particles and varying the remaining parameters using a grid search. A major achievement that is not discussed in the paper was a computationally efficient computer program that accurately approximates the maximum of the log-likelihood function in feasible time. A key component here was to control the lowering of the parameter driving the simulated annealing used for iterating the particle positions.

In a validation study, silica particles were simulated by the Poisson point process model and micrographs were generated using a power function with chosen fixed parameters. Not only were the shape parameters of the power function estimated correctly, but also the iterated particle positions showed a good fit. Finally, the method was evaluated on experimental micrographs and we showed that a power function performs statistically significantly better than a linear function. As a result, on fitting the parameters for the intensity power function, a non-unique solution to the three-dimensional particle positions and therewith an estimate for the mass thickness of the silica are obtained. This result is an important step towards a full three-dimensional particle position reconstruction.

This paper is co-authored with Matias Nordin, Christoffer Abrahamsson, Charlotte Hamngren Blomqvist, Magnus Röding, Eva Olsson, Magnus Nydén as well as Mats Rudemo and was published in Journal of Microscopy 253(2):166-170, 2014 (Nordin et al., 2014).

Paper II: From static micrographs to particle aggregation dynamics in three dimensions

In Paper I, we developed a method for estimating the mass thickness of nano sized (20 nm) silica particle gel samples from high angle annular dark-field scanning transmission electron micrographs. As a result, we obtained estimates of mass thickness of the silica at each pixel. However, the exact position of each particle in the direction of the electron beam within the sample was not obtained. For such a complete three-dimensional reconstruction of the particle positions, the connectivity between the particles and, hence, the aggregation dynamics involved have to be understood. In this study, the diffusion limited and the more general reaction limited cluster aggregation process are evaluated exactly for this purpose. A quantitative comparison of experimental micrographs to cluster aggregation simulations is the major part in our developed method of how to study the probability of aggregation assumed to drive the aggregation of the nanoparticles. A first component in our method is a micrograph simulation step using the relationship between mass thickness and intensity discussed in Paper I, but here to model the intensity in simulated micrographs. Subsequently, particles are detected by a newly composed particle detection algorithm based on standard tools from image analysis. Finally, the resulting point patterns of experimental and artificial particle centers are compared by common summary functions from spatial statistics and more specific summary functions for cluster analysis. One of these cluster analysis functions is based on the size of a cluster and was developed in this work.

In a least square approach collecting all information from the different summary functions, we drew a combined inference on the probability of aggregation that can be associated with the gel samples studied. All in all, we showed that different aggregation scenarios capture different structure characteristics of the gel samples, however, overall a very small probability of aggregation (<0.0001) seems most suitable for modeling the silica particle aggregation.

This paper is co-authored with Aila Särkkä, Mats Rudemo, Charlotte Hamngren Blomqvist, Eva Olsson, Christoffer Abrahamsson as well as Matias Nordin, and is intended for the Journal of Microscopy.

5.2 Paper III: Polymer blended films

Paper III: Characterization of pore structure of polymer blended films used for controlled drug release

Polymer blended films are often used as coatings in oral controlled drug release formulations, where the structure of the coating governs the release mechanism. In this work, a blend of two polymers is studied, where only one is water-permeable and acts as a pore former. On the attempt of understanding and controlling the release mechanism in such porous films, a characterization of the pore space becomes vital. Furthermore, the motivation for this study was a difference in permeability found between two films with different polymer viscosities, but nearly the same leakage measurements of the pore forming polymer. Hence, the question arose in which pore characteristics the pore structures differ within these two films.

In this study, two-dimensional scanning electron microscopy images of film cross-sections were available. After merging images from the same sample and having achieved a reasonable segmentation of the two polymer phases, we conducted an image analysis on the size and shape of the pores. Since results from pore size analyzes were already obtained in related studies, we focused on investigating and comparing different pore shape measures. An analysis of variance of all considered pore characteristics indicated a statistically significant difference between the two films in the number of branching and endpoints of the pore skeleton. Consequently, we found that the more permeable film seems to have a better pore connectivity due to more elongated shapes. This conclusion was in line with hypotheses developed during experiments, which had not been deduced from a statistical analysis before.

This paper is co-authored with Helene Andersson, Anna Jansson, Anette Larsson, Eva Olsson as well as Aila Särkkä, and is intended for the Journal of Controlled Release.

6 Future work

A natural continuation of the work presented in this thesis is to go from a two-dimensional characterization of materials to their three-dimensional characterization and reconstruction. For a complete three-dimensional reconstruction of the particle positions from micrographs of colloidal nanoparticle gel samples, the results from Paper I and Paper II can be combined. Here, a three-dimensional pore space analysis similar to the two-dimensional pore characterization introduced in Paper III can be conducted. Such an extension to a three-dimensional pore shape analysis is straightforward in theory, but requires more advanced image analysis techniques. Combining the results from Paper III and a three-dimensional pore shape analysis, a statistical model can be constructed also for polymer blended films based, for instance, on marked point processes.

Finally, three-dimensional models can be validated by comparing mass transport simulations through generated structures and experimentally obtained measurements from real materials. All in all, a virtual design framework can be set up for characterization, reconstruction and simulation of mass transport properties of different materials.

References

Atherton, T. and Kerbyson, D. Size invariant circle detection. *Image and Vision Computing*, 17:795–803, 1999. doi: 10.1016/S0262-8856(98)00160-7.

Cowie, J. *Polymers: Chemistry and Physics of Modern Materials*. CRC Press, Cheltenham, 1 edition, 1991.

Cussler, E.L. *Diffusion: Mass Transfer in Fluid Systems*. Cambridge University Press, Cambridge, 2 edition, 1997.

de Kruif, K., Hoffmann, M., van Marle, M., van Mil, P., Roefs, S., Verheul, M., and Zoon, N. Gelation of proteins from milk. *Faraday Discussions*, 101(1):185, 1995. doi: 10.1039/fd9950100185.

Einstein, A. Über die von der molekularkinetischen Theorie der Wärme geforderte Bewegung von in ruhenden Flüssigkeiten suspendierten Teilchen. *Annalen der Physik*, 322 (8):549–560, 1905. doi: 10.1002/andp.19053220806.

Glasbey, C. and Horgan, G. *Image Analysis for the Biological Sciences*. John Wiley and Sons, Ltd, Chichester, 1995.

Grimmett, G. and Stirzaker, D. *Probability and Random Processes*. Oxford University Press, Oxford, 3 edition, 2001.

Illian, J., Penttinen, A., Stoyan, H., and Stoyan, D. *Statistical Analysis and Modelling of Spatial Point Patterns*. John Wiley and Sons, Ltd, Chichester, 2008.

Khan, M. N., Auerbach, S., and Monson, P. Lattice model for silica polymerization: Monte Carlo simulations of the transition between gel and nanoparticle phases. *The Journal of Physical Chemistry. B*, 118(37):10989–99, 2014. doi: 10.1021/jp504961q.

Klemm, D., Heublein, B., Fink, H.-P., and Bohn, A. Cellulose: Fascinating Biopolymer and Sustainable Raw material. *Angewandte Chemie International Edition*, 44:3358–3393, 2005. doi: 10.1002/anie.200460587.

Lam, L. and Lee, S.W. Thinning Methodologies - A Comprehensive Survey. *IEEE Transactions on Pattern Analysis and Machine Intelligence*, 14(9):869–885, 1992. doi: 10.1109/34.161346.

Marucci, M., Arnehed, J., Jarke, A., Matic, H., Nicholas, M., Boissier, C., and von Corswant, C. Effect of the manufacturing conditions on the structure and permeability of polymer films intended for coating undergoing phase separation. *European Journal of Pharmaceutics and Biopharmaceutics*, 83(2):301–306, 2013. doi: 10.1016/j.ejpb.2012.09.020.

Nordin, M., Abrahamsson, C., Hamngren Blomqvist, C., Häbel, H., Röding, M., Olsson, E., Nydén, M., and Rudemo, M. Estimation of mass thickness response of embedded aggregated silica nanospheres from high angle annular dark-field scanning transmission electron micrographs. *Journal of Microscopy*, 253(2):166–70, 2014. doi: 10.1111/jmi.12107.

Otsu, N. A Threshold Selection Method from Gray-Level Histograms. *IEEE Transactions on Systems, Man, and Cybernetics*, 9(1):62–66, 1979. doi: 10.1109/TSMC.1979.4310076.

Pennycook, S., Lupini, A., Varela, M., Borisevich, A., Peng, Y., Oxley, M., and Chisholm, M. *Scanning microscopy for nanotechnology: techniques and applications*, chapter Scanning transmission electron microscopy for nanostructure characterization, pages 152–191. Springer, 2006.

Penrose, M. *Random Geometric Graphs*. Oxford University Press, Oxford, 2003.

Rajala, T. Spatial point processes and graph based statistical features. *2000 Mathematics Subject Classification*, Preprint 385, 2010.

Sakellariou, P. and Rowe, R. C. Interactions in cellulose derivative oral drug delivery. *Progress in Polymer Science*, 20:889–942, 1995. doi: 10.1016/0079-6700(95)00008-4.

Schantz Zackrisson, A., Martinelli, A., Matic, A., and Bergenholtz, J. Concentration effects on irreversible colloid cluster aggregation and gelation of silica dispersions. *Journal of Colloid and Interface Science*, 301(1):137–44, 2006. doi: 10.1016/j.jcis.2006.04.066.

Stoyan, D., Kendall, W., and Mecke, J. *Stochastic Geometry and its Applications*. John Wiley and Sons, Ltd, Chichester, 2 edition, 1995.